V. 5. Improvement of The Performance of Tohoku Microbeam System

Matsuyama S.[1], Ishii K.[1], Tsuboi S.[1], Hashimoto Y.[1], Kawamura Y.[1], Yamanaka K.[1], Watanabe M.[1], Ohkura S.[1], Fujikawa M.[1], Catella G.[1], Fujiki K.[1], Hatori Y.[1], Hamada N.[1], Fujiwara M.[1], Kikuchi Y.[1], and Yamazaki H.[2]

[1]*Department of Quantum Science and Energy Engineering, Tohoku University*
[2]*Cyclotron and Radioisotope Center, Tohoku University*

Introduction

High-energy ion microbeams are versatile tools for analyses in a microscopic region[1-3]. A microbeam system was installed at Dynamitron laboratory at Tohoku University in July 2002 for biological applications with sub-micrometer resolution[4]. Beam spot of 0.4×0.4 μm^2 at a beam current of several tens of pA has been produced[5]. The analysis system has also been developed and is applicable to simultaneous in-air/in-vacuum PIXE, RBS, SE, and STIM analyses[6,7], and 3D μ-CT[8-10]. In our set-up, μ-PIXE/RBS analyses demand beam currents of ca. 100 pA, which restricts the spatial resolution to around 1×1 μm^2. Recently, higher spatial resolution down to several hundred nm is required in aerosol studies. In in-vivo 3D imaging using 3D PIXE-μ-CT, we faced two problems: the reconstructed image was blurred due to the movements of the specimen and the long measurement time of several hours weakened the specimen. Thus beam currents higher than several hundred pA are required in 3D PIXE-μ-CT applications. Beam brightness must be increased to meet these requirements. In the previous study, the terminal equipment and an acceleration tube of the Dynamitron accelerator were upgraded. However obtained beam brightness is lower than expected and than that of previous system. As for microbeam system, parasitic field contamination should be eliminated to obtain submicron resolution. While the parasitic field contamination of the system was greatly reduced in the previous study, contamination of the skew sextupole field of ca. 0.1% was still remaining. While the effect of sextupole contamination could be reduced by reducing a half divergence into the quadrupole lenses, which also reduces beam current and is undesirable in our purpose.

In this study, optimization and modification of the ion source and microbeam system were performed to improve the performance.

Improvement of the System

Ion Source

The terminal equipment comprises a duoplasmatron ion source along with an extractor, an Einzel lens, an ExB filter, a pulsing system, and a gap lens, which were provided by National Electrostatics Corporation (NEC), USA. Technical details of the system were presented in previous paper[11]. The ion source is expected to produce ca. 10 mA H_1^+ beams, with beam emittance of 2.1 mm· mrad· $MeV^{1/2}$ (specification). Both values are better than those of the previous ion source. However, beam brightness after passing the energy analyzing system was 0.44 $pA \cdot \mu m^{-2} \cdot mrad^{-2} \cdot MeV^{-1}$ for H_1^+ beams at half divergence of 0.07 mrad, which was lower than expected and than those of the previous ion source.

In the installation of the system, the ion source was modified to achieve longer lifetime, which is the most important property for an ion source used in the single-ended machine. Figure 1 shows the duoplasmatron ion source and anode aperture assemblies. A LaB_6 filament (C2B, Denka Co. Ltd.) was used instead of an uncoated tungsten filament (0.9 mm diameter) supplied from NEC. A 0.1-mm-diameter anode aperture assembly (expansion cup) made of soft magnetic iron was replaced by different one with 0.3-mm-diameter anode aperture insert made of tungsten (Fig. 1(a)). Outer diameters of the insert are 9.5 mm and 8 mm for source and extractor sides, respectively. The shape and dimension of the assembly are identical to those of original design except for diameter of the aperture. Lower performance might be related to these modifications. Ion beams are extracted through an anode aperture of the duoplasmatron ion source. Shape and diameter of the anode aperture affects beam property. The anode aperture also has functions to shield magnetic field from the source and to close magnetic circuit. Since outer diameters of the previous anode aperture insert were 8 mm and 9.5 mm, shielding of the magnetic field might be insufficient. For this reason, outer diameter of the aperture insert was reduced down to 4 mm (Fig. 1(b)).

Microbeam System

The microbeam system was developed in collaboration with Tokin Machinery Corp and was described precisely in previous papers[4,5]. A high-resolution energy analysis

system is installed upstream of the microbeam line. The microbeam line comprises a quadrupole doublet and three slit systems: micro-slit, divergence-defining slit, and baffle slit. The total length of the line is ca. 7 m. The demagnification factors were 35.4 and 9.2 for horizontal and vertical directions, respectively, which were the highest values in our system[5]. At fist, parasitic field contamination from microbeam line components, restricted the resolution. In order to reduce parasitic field contamination, some of those components were replaced or redesigned. However sextupole field contamination superimposed onto the quadrupole field in the horizontal focusing was still remaining. The rigid support of the line made of steel and beam ducts made by stainless steel (SUS304) might be the source. Since the distance between beam line and the rigid support is ca. 25 cm, magnetic field contamination from the support might be dipole and will not affects beam sizes. Strong multipole field contamination from a stainless beam duct (SUS316, outer diameter 10 mm) was reported[12]. In our system, the minimum diameter of the beam ducts from micro-slit to baffle-slit is ca. 60 mm and might not cause multipole contamination. However, diameter of the beam ducts from baffle-slit to the target chamber was rather small and might cause multipole contamination. While a beam duct in the quadrupole doublet is the smallest diameter and is made of aluminum, other parts are made of stainless steel (SUS304). Especially, a beam scanner camber was made of stainless steel and was asymmetric design. The outer diameter was 52 mm. The beam scanner chamber was redesigned and was made by aluminum. The chamber was cut as one body from a single aluminum piece to reduce volume. Thus, the demagnification factors are further improved to 40.8 and 9.8 for horizontal and vertical directions, respectively. A bypass line made by stainless steel, which had been used to reduce pressure in the target chamber, laid in parallel to the beam line on the quadrupole doublet. The bypass line was also removed. Realignment of the line was carried out. The target chamber sunk 1.5 mm, which resulted from the increase of mass of analysis system.

The micro-slit comprises two wedge-shaped slits supplied from Technisches Büro S. Fischer, Germany, which were made from 4-mm-diameter and 15 mm long tungsten carbide cylinders whose spacing was increasing linearly from 0–150 μm. Aluminum body of the micro-slit was eroded after several high-current experiments. In order to withstand heat loading to the micro-slit in the high current application, it was redesigned. The diameter of tungsten carbide cylinders set to 5 mm. Pre-slits and a part of the casing were made of tantalum. To extend beam size range from 0 to 6 μm, the spacing is adjustable from 0 to

250 μm corresponding to a longitudinal motion of 0-24 mm.

Performance

Beam brightness

The beam brightness is of primary importance to focus the beam down to sub-micrometer scale with sufficient beam current and has to be measured after passing through the energy analysis system. Then the system's beam brightness was estimated from the target current measurement in the microbeam with the micro-slit opening fixed and divergence defining slit one varied. The micro-slit widths were set at 74×14 μm^2, which correspond to beam spot size of 1.5×1.5 μm^2. Slit opening of the analyzing system was set at 0.6 mm, which is the conventional opening in the analysis mode. Energy resolution of the analyzing system is estimated to be 2.0×10^{-4} $\triangle$P/P. Figure 2 shows the measured beam brightness before and after modifications. The beam brightness after changing the anode aperture is 0.5 $pA\cdot\mu m^{-2}\cdot mrad^{-2}\cdot MeV^{-1}$ at a half divergence of 0.2 mrad and is 1.6 times higher than before.

As for the microbeam line, the beam brightness became 1.0 $pA\cdot\mu m^{-2}\cdot mrad^{-2}\cdot MeV^{-1}$ at a half divergence of 0.2 mrad and 1.7 times higher than that of the previous ion source. Considering the brightness and the magnification, obtainable target current will be 200 and 900 pA for beam spot sizes of 1.0×1.0 and 2.0×2.0 μm^2, respectively. Normal beam brightness at a half divergence of 0.07 mrad is 1.6 $pA\cdot\mu m^{-2}\cdot mrad^{-2}\cdot MeV^{-1}$ which is only 1.6 times higher than that at a half divergence of 0.2 mrad. It means that the beam intensity distribution in the phase space is uniform.

The ion source and the anode aperture have worked more than 2800 and 1800 hrs, respectively, without changing beam properties and are still running. The modification of the source meets both the lifetime and the performance. However, the brightness is still lower than that expected from the source. Because the anode aperture diameter also affects the brightness, aperture optimization should be done.

Field contamination

In the grid shadow method, the beam is focused on the image plane, where a fine mesh grid is placed, by a single quadrupole lens and casts shadow pattern on a scintillator downstream[14,15]. The shadow pattern is influenced strongly by lens aberration and parasitic field contaminations of the microbeam system. Geometry of shadow pattern

measurement was the same as the previous measurements[5]. In this measurement, we set the divergence to ±0.35 mrad, which is the largest acceptance of the microbeam line and smaller than that from the accelerator. Figure 3 shows the measured grid shadow patterns for the two quadrupole lenses with a 3 MeV proton beam. The measured shadow patterns are straight and are not deformed. Since the minimum detectable limit corresponds to approximately 0.05% for sextupole field contamination superimposed onto the quadrupole field[5] calculated by the beam optics computer codes, PRAM and OXTRACE[3], field contamination is less than 0.1%. In the previous study, it was suspected that the cancellation of excitation current of the quadrupole is not perfect[5]. In this study, no modification was made to the quadrupole. Therefore, the contamination came from the beam scanner and a part of beam line. The Tohoku microbeam system has a capability to focus the beam down as theoretical even in the large half divergence into the quadrupole.

Beam Size

The beam spot size was obtained by fitting the measured line profiles of X-rays from the Au mesh (2000 lines/inch)[6]. Slit opening of the analyzing system was set at 0.6 mm and the half divergence was set at 0.2 mrad, which is the conventional opening in the analysis mode. Beam spot sizes diminished concomitant with the object slit sizes and were saturated with ca. 500×500 nm^2, which might be the effect of chromatic aberration.

Figure 4 shows typical example of secondary electron image of carbon steel oxidized under dynamic condition[16]. MS widths were set at 20×5 μm^2, which correspond to beam spot size of 0.5×0.5 μm^2 at the half divergence of 0.2 mrad. Changes in secondary electron intensities along grain boundary are clearly seen. From the comparison with the marker indicated in the figure, the spatial resolution is ca. 0.5×0.5 μm^2 and consistent with the estimation. Simultaneous PIXE/RBS analysis could be done.

In the 3D PIXE-μ-CT experiments, beam current of several hundred pA are routinely obtained with the beam spot sizes of ca. 2×2 μm^2 and *in-vivo* 3D imaging is realized. These results will be presented elsewhere.

Conclusions

In order to improve the performance of Tohoku microbeam system, optimization and modification of the ion source and microbeam system were performed. The anode aperture of the duoplasmatron ion source was redesigned and installed. The object slits of

the microbeam line was redesigned to withstand higher beam current. The parasitic field contamination of the system was reduced down to less than 0.05% by replacing the beam scanner and a part of beam duct. The beam brightness of the system was 1.0 $pA \cdot \mu m^{-2} \cdot mrad^{-2} \cdot MeV^{-1}$ at the half divergence of 0.2 mrad and was 1.7 times higher than that of the previous ion source. Considering the brightness and the magnification, obtainable target current will be 200 and 900 pA for beam spot sizes of 1×1 and 2×2 μm^2, respectively at the half divergence of 0.2 mrad. The ion source and the anode aperture have worked more than 2800 and 1800 hrs, respectively, without changing beam properties and are still running. The modification of the source meets both the lifetime and the performance. Deformation of MS is completely reduced by the modification even in the beam load of several μA. Both resolution and beam currents are sufficient for our application and Tohoku microbeam system has been operated routinely for simultaneous in-air/in-vacuum PIXE, RBS, SE, and STIM analyses and for *in-vivo* 3D PIXE-μ-CT imaging.

Acknowledgement

The authors would like to acknowledge the assistance of Fujisawa M. for maintenance and operation of the Dynamitron accelerator. The authors would like to thank Mr. Nagaya T. and Komatsu K., for the modification of the accelerator and microbeam system.

References

1) Watt F., Grime G.W., Principal and Applications of High-energy Ion Microbeams, Adam Hilger, Bristol, 1987.
2) Johansson S.A.E., Campbell J.L., Malmqvist K.G., Particle-Induced X-ray Emission Spectrometry (PIXE), John Wiley and Sons, N.Y., 1995.
3) Breese M.B.H., Jamieson D.N., King P.J.C., Materials Analysis using Nuclear Microprobe, John Wiley and Sons, N.Y., 1995.
4) Matsuyama S., Ishii K., Yamazaki H., Sakamoto R., Fujisawa M., Amartaivan Ts., Ohishi Y., Rodriguez M., Suzuki A., Kamiya T., Oikawa M., Arakawa K., Matsumoto N., Nucl. Instr. and Meth. **B 210** (2003) 59.
5) Matsuyama S., Ishii K., Yamazaki H., Kikuchi Y., Inomata K., Watanabe Y., Ishizaki A., Oyama R., Kawamura Y., Yamaguchi T., Momose G., Nagakura Takahashi M.M., Kamiya T., Nucl. Instr. and Meth. **B 260** (2007) 55.
6) Matsuyama S., Ishii K., Yamazaki H., Barbotteau Y., Amartaivan Ts., Izukawa D., Hotta K., Mizuma, K., Abe S., Oishi Y., Rodriguez M., Suzuki A., Sakamoto R., Fujisawa M., Kamiya T., Oikawa M., Arakawa K., Imaseki H., Matsumoto N., Int. J. of PIXE **14** (1&2) (2004) 1.
7) Matsuyama S., Ishii K., Abe S., Ohtsu H., Yamazaki H., Kikuchi Y., Amartaivan Ts., Inomata K., Watanabe Y., Ishizaki A., Barbotteau Y., Suzuki A., Yamaguchi T., Momose G., Imaseki H., Int. J. of PIXE **15** (1&2) (2005) 41.
8) Ishii K., Matsuyama S., Yamazaki H., Watanabe Y., Yamaguchi T., Momose G., Amartaivan Ts., Suzuki A., Kikuchi Y., and Galster W., Int. J. of PIXE **15** (3&4) (2005) 111.
9) Ishii K., Matsuyama S., Yamazaki H., Watanabe Y., Kawamura Y., Yamaguchi T., Momose

G., Kikuchi Y., Terakawa A., Galster W., Nucl. Instr. and Meth. **B 249** (2006) 726.
10) Ishii K., Matsuyama S., Watanabe Y., Kawamura Y., Yamaguchi T., Oyama R., Momose G., Ishizaki A., Yamazaki H., Kikuchi Y., Nucl. Instr. and Meth. **A 571** (2007) 64.
11) Matsuyama S., Ishii K., Fujisawa M., Kawamura Y., Tsuboi S., Yamanaka K., Wtanabe M., Hashimoto Y., Ohkura S., Fujikawa M., Nagaya T., Komatsu K., Yamazaki H., Kikuchi Y., Nucl. Instr. and Meth. **B 267** (2009) 2060.
12) Jamieson D.N., Nucl Instr and Meth. **B 181** (2001) 1.
13) Roland Szymanski, David N. Jamieson, Nucl. Instr. and Meth. **B 130** (1997) 80.
14) Jamieson D.N., Legge G.J.F., Nucl. Instr. and Meth. **B 29** (1987) 544.
15) Jamieson D.N., Zhu J., Mao Y., Lu R., Wang Z., Zhu J., Nucl. Instr. and Meth. **B 104** (1995) 86.
16) Matsuyama S., Ishii K., Fujiwara M., Kikuchi Y., Nakhostin M., Kawamura Y., Watanabe M., Ohkura S., Hashimoto Y., Fujikawa M., Catella G., Fujiki K., Hatori Y., Hamada N., Tanino S., Abe H., Watanabe Y. Yamazaki H., Int. J. of PIXE **19** (1&2) (2009) 61.

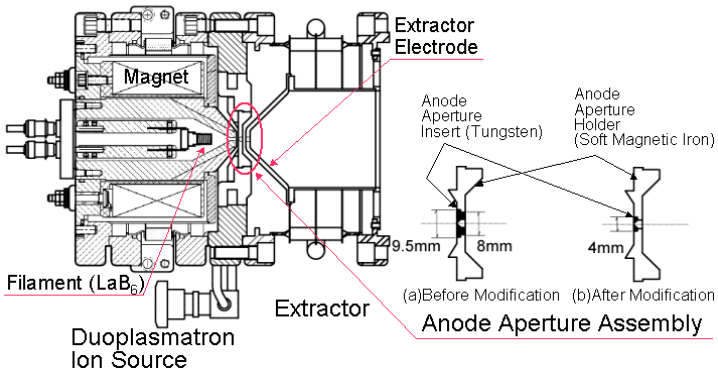

Figure 1. Duoplasmatron Ion Source and Anode Aperture Assembly.

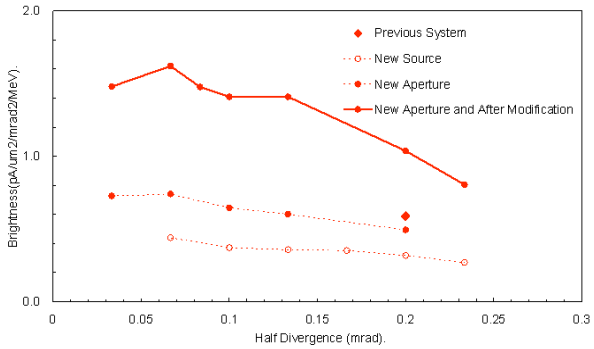

Figure 2. Measured beam brightness.

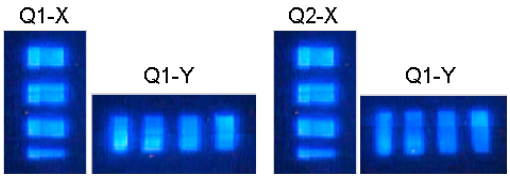

Figure 3. Measured Grid Shadow Pattern.

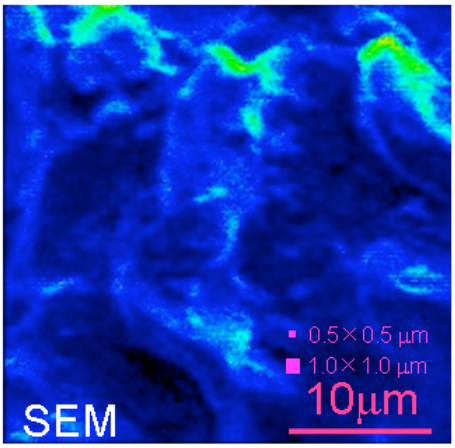

Figure 4. Secondary Electron Image of Carbon Steel Oxidized under Dynamic Condition.